Eur. Phys. J. D **7**, 567–571 (1999)

THE EUROPEAN PHYSICAL JOURNAL D

EDP Sciences

Dynamics of BF_4^- anion reorientation in the spin-crossover compound $[Fe(1-n-propyl-1H-tetrazole)_6](BF_4)_2$ and in its Zn^{II} analogue

M. Bokor[1,2,a], T. Marek[1], K. Tompa[1], P. Gütlich[3], and A. Vértes[2]

[1] Research Institute for Solid State Physics and Optics, Hungarian Academy of Sciences, pob. 49, 1525 Budapest, Hungary
[2] Department of Nuclear Chemistry, Eötvös University, Budapest, Hungary
[3] Institut für Anorganische Chemie und Analytische Chemie, Johannes-Gutenberg-Universität Mainz, Germany

Received 09 February 1999 and Received in final form 14 June 1999

Abstract. ^{19}F and ^{11}B spin-lattice relaxation times were measured in $[Zn(ptz)_6](BF_4)_2$ (ptz = $1-n-$propyl$-1H-$tetrazole) and in the spin-crossover compound $[Fe(ptz)_6](BF_4)_2$. For both compounds BF_4^- anion reorientation is active above 50 K. For $[Zn(ptz)_6](BF_4)_2$, the anion-reorientation dynamics is different in the temperature regions of 50–90 K, 90–120 K, and above 150 K; between 120 and 150 K it changes rapidly reflecting a structural change. In $[Fe(ptz)_6](BF_4)_2$ the mechanism for the paramagnetic relaxation involving the ^{19}F nuclei is found to be of the diffusion-limited type according to the theory of Lowe and Tse. The present results prove that the spin-crossover takes place in a dynamic surrounding and not in a static crystal lattice.

PACS. 33.15.Vb Correlation times in molecular dynamics – 33.15.Hp Barrier heights (internal rotation, inversion, rotational isomerism, conformational dynamics) – 33.25.+k Nuclear resonance and relaxation

1 Introduction

In studies of the molecular motions and structural changes of a compound showing thermally induced spin transition [1], the question always arises whether the spin transition induces a change of molecular structure and motions or inversely. Our presently studied example is the hexakis($1-n-$propyl$-1H-$tetrazole)iron(II) bistetrafluoroborate ($[Fe(ptz)_6](BF_4)_2$). This compound undergoes a thermal spin transition with hysteresis of *ca.* 7 K width near $\sim$ 130 K [2–4] accompanied by a crystallographic phase transition [5].

The exchange of the central iron(II) ions to zinc(II) has almost no effect on the structure and so a perfect model is gained for our purpose, which lacks the very strong effects of unpaired electrons. ^1H line-shape temperature dependence [6,7] revealed that in both compounds the activation of different intramolecular motions of the cation complex appears at the same temperatures. ^1H spin-lattice relaxation time curves for the zinc cation complex [6] indicated three different types of reorientation of the propyl group and a transient region where a small structural rearrangement perturbs the molecular dynamics. Positron annihilation (2D ACAR) studies [8] suggested a major role of the anions there. ^{19}F and ^{11}B spin-lattice relaxation time (T_1) measurements were carried out to get a more detailed picture on the changes of the reorientations of the propyl group and the anion. The clearing up of the problem that the changes of the lattice dynamics is responsible for or induced by the spin transition will provide a new perspective and deeper insight in the field of the solid state spin transition phenomenon.

2 Experimental

2.1 Sample preparation

The $1-n-$propyl$-1H-$tetrazole (ptz) ligand was prepared as described by Franke *et al.* [2]. $[Fe(ptz)_6](BF_4)_2$ and $[Zn(ptz)_6](BF_4)_2$ were prepared by the method of Poganiuch *et al.* [9]. The crude (polycrystalline) products were recrystallized from nitromethane to obtain single crystals. For the NMR measurements polycrystalline samples were used.

2.2 NMR Spectroscopy

T_1 for ^{19}F was measured at 83.5 and 29.0 MHz, and for ^{11}B at 29.0 MHz on a SMIS spectrometer by using the saturation recovery and the inversion recovery methods. The stability of frequency and magnetic field was better than $\pm 1 \times 10^{-6}$. The temperature was controlled by an open-circle Oxford cryostat and an Oxford ITC4 temperature controller using He gas flow. The uncertainty

[a] e-mail: mbokor@power.szfki.kfki.hu

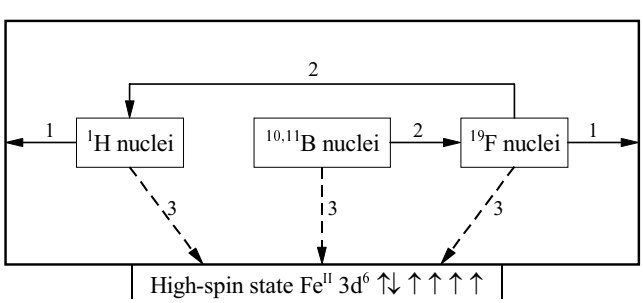

Fig. 1. Spin interactions reflected by T_1 for [Zn(1–propyl–1H–tetrazole)$_6$](BF$_4$)$_2$ and [Fe(1–propyl–1H–tetrazole)$_6$](BF$_4$)$_2$; 1: direct spin-lattice interaction, 2: interaction between heteronuclear spins, 3: nuclear spin diffusion (only present in the iron compound).

of the temperature control was less than 1 K. The cooling rate was about 1 K min^{-1}.

3 Results and discussion

Figure 1 shows the dominant relaxation channels among ^{1}H, ^{19}F, ^{11}B, and ^{10}B nuclei and the lattice, contributing to T_1. Direct (dipolar) interactions with the lattice are represented by paths 1. ^{19}F nuclei relax also by energy transfer to the ^{1}H nuclei (path 2) which manifests in nonexponential relaxation of magnetization. In the relaxation of the ^{1}H nuclei, the heteronuclear interaction has no detectable effect on T_1 (exponential relaxation of magnetization [6,10]). Boron nuclei relax almost exclusively by energy transfer to the fluorine nuclei (path 2). Their direct interaction with the lattice is not effective. When high-spin state Fe^{II} ions are present in [Fe(ptz)$_6$](BF$_4$)$_2$, all four kinds of nuclei undergo spin diffusion caused by the unpaired electron spins (paths 3) and paramagnetic electron spin relaxation is active.

3.1 [Zn(ptz)$_6$](BF$_4$)$_2$

Figure 2 shows ^{19}F T_1 and ^{11}B T_1 observed in the temperature ranges 40–300 K and 50–337 K, respectively. The data for ^{19}F, measured at two different frequencies, show the following trends.

(a) The gradient of the T_1 curve is smaller below 50 K than between 50 and 70 K (Fig. 3).
(b) Between 55 and 85 K, a T_1 minimum is detected (Fig. 2).
(c) In the temperature range of 90 to 120 K T_1 is the same for both resonance frequencies.
(d) Between 120 and 150 K T_1 shows local minimum.
(e) Above 150 K, relaxation times are changing smoothly. For the data recorded at lower resonance frequency, a shallow minimum is detected around 225 K.

The boron relaxation times follow the same trend except for region (d) where T_1 changes smoothly with the temperature. In region (e) the minimum is more expressed for boron than for 29.0 MHz fluorine T_1.

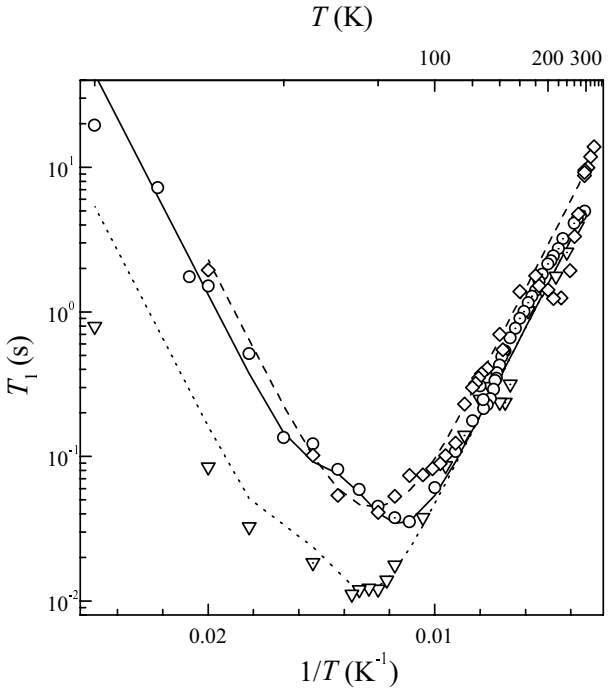

Fig. 2. ^{19}F and ^{11}B spin-lattice relaxation times for [Zn(1–propyl–1H–tetrazole)$_6$](BF$_4$)$_2$. (▽): ^{19}F T_1 at 29.0 MHz; (○): ^{19}F T_1 at 83.5 MHz; (◇): ^{11}B T_1 at 29.0 MHz; symbols with dot center: single exponential relaxation; lines: fitted theoretical curves, equations (4–6).

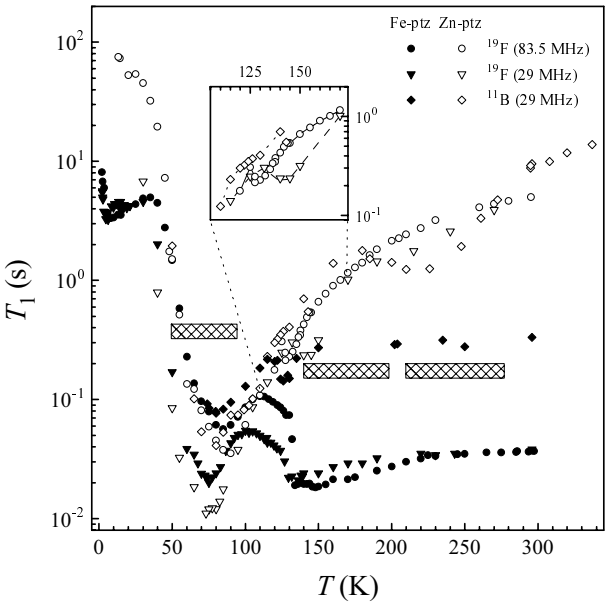

Fig. 3. ^{19}F and ^{11}B spin-lattice relaxation times for [Zn(1–propyl–1H–tetrazole)$_6$](BF$_4$)$_2$ and [Fe(1–propyl–1H–tetrazole)$_6$](BF$_4$)$_2$. T_1 for the iron compound is dominated by the magnetic field of the high-spin state electron structure of Fe^{II} ions above 110 K. Insert: magnified plot of fluorine and boron T_1; note the sharp changes in trends. Boxes: regions of ^{1}H T_1 motional minima; the lowest temperature one is attributed to reorientation of CH$_3$ groups and the others to other reorientations of the propyl sidechaines [10].

Analyzing fluorine and boron relaxation times in region (b), the minimum can be explained as caused by the reorientation of the BF_4^- anions. Below 150 K, the recovery of the longitudinal fluorine magnetization is nonexponential what is considered as resulting from cross relaxation between protons and fluorine nuclei (path 2 in Fig. 1). T_1 values of both spins can be expressed *via* the following pair of coupled differential equations [11]

$$\frac{\mathrm{d}\langle M_z^{\mathrm{F}}\rangle}{\mathrm{d}t} = -R_{\mathrm{F}}\left(\langle M_z^{\mathrm{F}}\rangle - M_0^{\mathrm{F}}\right) - R_{\mathrm{FH}}\left(\langle M_z^{\mathrm{H}}\rangle - M_0^{\mathrm{H}}\right),$$
$$\frac{\mathrm{d}\langle M_z^{\mathrm{H}}\rangle}{\mathrm{d}t} = -R_{\mathrm{HF}}\left(\langle M_z^{\mathrm{F}}\rangle - M_0^{\mathrm{F}}\right) - R_{\mathrm{H}}\left(\langle M_z^{\mathrm{H}}\rangle - M_0^{\mathrm{H}}\right), \quad (1)$$

where $\langle M_z^{\mathrm{I}}\rangle$ and $\langle M_0^{\mathrm{I}}\rangle$ are the z components of the magnetization for I = ^{19}F or ^{1}H at time t and at thermal equilibrium, respectively. The solution of equation (1) for a 90°–t–90° pulse sequence applied to ^{19}F yields [11]

$$\frac{\langle M_z^{\mathrm{F}}\rangle - M_0^{\mathrm{F}}}{M_0^{\mathrm{F}}} = \frac{R_{\mathrm{F}} - R''}{R'' - R'}\mathrm{e}^{-tR'} + \frac{R_{\mathrm{F}} - R'}{R' - R''}\mathrm{e}^{-tR''}. \quad (2)$$

The observed relaxation rates R' and R'' are eigenvalues of the relaxation matrix

$$R = \begin{bmatrix} R_{\mathrm{F}} & R_{\mathrm{FH}} \\ R_{\mathrm{HF}} & R_{\mathrm{H}} \end{bmatrix}. \quad (3)$$

$T_1 = R_{\mathrm{F}}^{-1}$ calculated by using equation (2), is shown in Figure 2. The recovery of the longitudinal ^{1}H [6,9] and ^{11}B magnetization were exponential above 40 K: $\mathrm{d}\langle M_z\rangle/\mathrm{d}t = -R(\langle M_z\rangle - M_0)$. The cross relaxation term in equation (1) for protons is so small that it could not be detected.

On the low temperature side (Fig. 2), ^{19}F T_1 shows a single minimum with a shoulder which also refers to a not negligible contribution of the R_{FH} term in equation (1). The general expression for the matrix element R_{F} of equation (3) may be written as [11]

$$R_{\mathrm{F}} = \frac{2}{3}\gamma_{\mathrm{F}}^2 \Delta M_{\mathrm{FF}} g(\omega_{\mathrm{F}}, \tau_{\mathrm{F}}) + \frac{1}{3}\gamma_{\mathrm{F}}^2 \sum \Delta M_{\mathrm{FB}} g_{\mathrm{F}}(\omega_{\mathrm{BF}}, \tau_{\mathrm{F}}) + \alpha\gamma_{\mathrm{F}}^2 \Delta M_{\mathrm{FH}} g_{\mathrm{F}}(\omega_{\mathrm{HF}}, \tau_{\mathrm{F}}) + \beta\gamma_{\mathrm{F}}^2 \Delta M'_{\mathrm{FH}} g_{\mathrm{F}}(\omega_{\mathrm{HF}}, \tau_{\mathrm{H}}). \quad (4)$$

The spectral density functions $g(\omega, \tau)$ are defined as follows:

$$g(\omega_i, \tau_i) = \frac{\tau_i}{1 + \omega_i^2\tau_i^2} + \frac{4\tau_i}{1 + 4\omega_i^2\tau_i^2}, \quad (5)$$

$$g_{\mathrm{F}}(\omega_{\mathrm{SF}}, \tau_j) = \frac{\tau_j}{1 + (\omega_{\mathrm{S}} - \omega_{\mathrm{F}})^2\tau_j^2} + \frac{3\tau_j}{1 + \omega_i^2\tau_j^2} + \frac{6\tau_j}{1 + (\omega_{\mathrm{S}} + \omega_{\mathrm{F}})^2\tau_j^2}, \quad (6)$$

where i and j denote ^{1}H or ^{19}F; S is ^{1}H, ^{10}B, or ^{11}B. The correlation times τ_i and τ_j change with temperature according to $\tau = \tau_0 \mathrm{e}^{E_{\mathrm{a}}/RT}$ (τ_0: correlation time at infinite temperature, E_{a}: activation energy). In equation (4), ΔM_{ij} is the contribution to the second moment of the ith nucleus, caused by its interactions with the jth nuclei, what is averaged out by the reorientations with the $g(\tau_k)$ that multiplies ΔM_{ij}. The second term in equation (4) is the summation for the two kinds of isotopes ^{10}B and ^{11}B. The coefficients of α and β are determined by depending on how the correlation functions are averaged by the motions.

Table 1. Calculated activation energies and correlation times for anion and methyl reorientation in [Zn(1–propyl–1H–tetrazole)$_6$](BF$_4$)$_2$ and [Fe(1–propyl–1H–tetrazole)$_6$](BF$_4$)$_2$.

Reorientation	E_a/kJ mol^{-1}	$\tau_0/10^{-12}$ s	$C_{ij}/10^9$ s^{-2}	
BF_4^- in [Zn(ptz)$_6$](BF$_4$)$_2$	5.35	1.05	1.1 (FF), 3.0 (^{11}BF), 2.4 (^{11}BF)	1.1 (^{10}BF) 0.31 (FH)
BF_4^- in [Fe(ptz)$_6$](BF$_4$)$_2$	5.20	1.19	0.78 (FF), 1.7 (^{11}BF), 1.4 (^{11}BF)	0.60 (^{10}BF) 0.19 (FH)
CH_3 [6] in [Zn(ptz)$_6$](BF$_4$)$_2$	3.90	3.18		

Equations (4–6) were employed to fit (Fig. 2) the fluorine T_1 data at 55 K $\leq T \leq$ 85 K. For boron T_1 data a formula similar to equation (4) but consisting only of cross terms (path 2 in Fig. 1) was employed in the same temperature range. Multipliers of the spectral density functions were merged into parameters C_{ij}. τ_{H} was determined from the minimum in proton T_1 formerly identified as resulting from CH_3 reorientation [6]. Activation energies, correlation times and C_{ij}-s determined from fitting the above equations to fluorine and boron relaxation times simultaneously are listed in Table 1. The uncertainty of the given parameters is characterized by the number of the digits. As expected, $\Delta M'_{\mathrm{HF}}$ proved to be negligible.

For the frequency independent part of the ^{19}F T_1 (region (c): 90–120 K), the measured T_1 values are consequently higher than the result of the calculations for 55 K $\leq T \leq$ 85 K. The average ^{19}F–^{1}H distances are suggested therefore to be different in this region. The activation energy E_{a} value evaluated from the gradient of the experimental T_1 curves is 5.84 kJ mol^{-1}, somewhat larger than the E_{a} calculated for the lower-temperature region. In region (d), around 130–140 K ^{19}F (at both frequencies) and ^{11}B T_1 curves show a broken trend (Figs. 2 and 3) what was also present in the ^{1}H T_1 temperature dependence [6]. The activation energy of the BF_4^- reorientation becomes lower (5.16 kJ mol^{-1}) above 150 K.

The above phenomena refer to changes of the dynamic structure at 130–140 K, what results in a different anion dynamics and activate new type of propyl-group reorientations.

The ^{11}B T_1 minimum in region (e), at 225 K (Figs. 2 and 3) can formally be described with large activation energy, rapid reorientation and small second moment reduction and it is thought to be of quadrupolar origin.

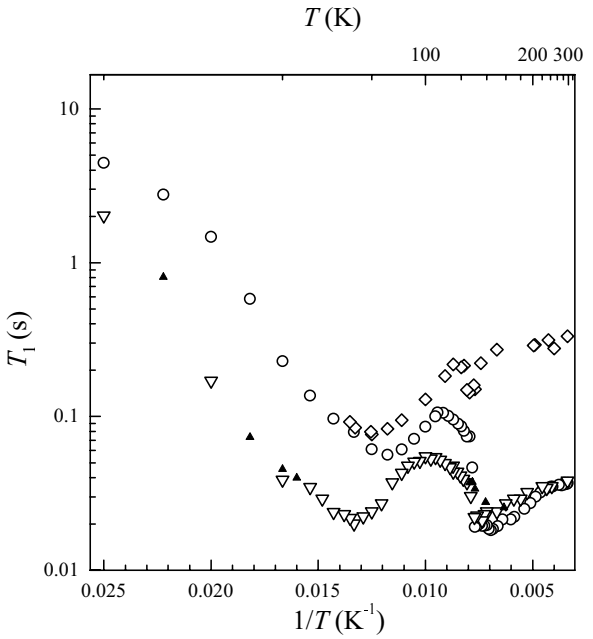

Fig. 4. ^{19}F and ^{11}B spin-lattice relaxation times for [Fe(1–propyl–1H–tetrazole)$_6$](BF$_4$)$_2$. Triangles: ^{19}F T_1 at 29.0 MHz ((▽) correspond to the cooling, (▲) to the heating direction); (○): ^{19}F T_1 at 83.5 MHz; (◇): ^{11}B T_1 at 29.0 MHz.

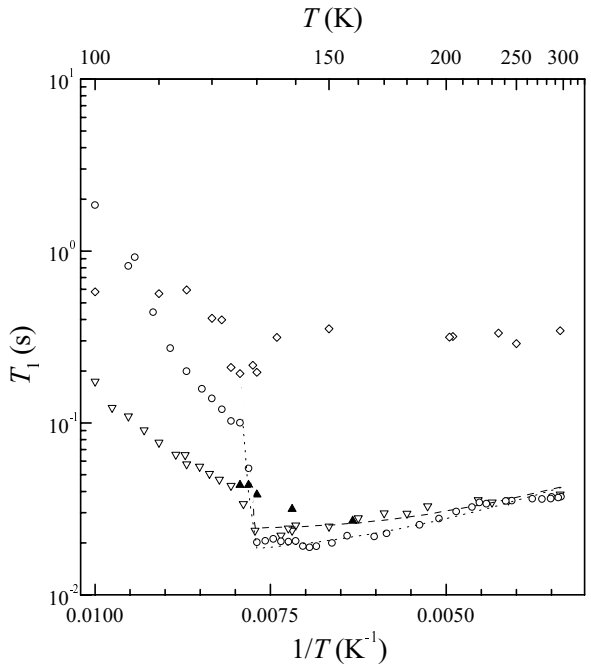

Fig. 5. Spin-lattice relaxation time calculated as $T_1^{-1} = T_{1,\mathrm{meas.}}^{-1} - T_{1,\mathrm{dip.}}^{-1}$, where the dipolar spin-lattice relaxation rate (estimated by the theoretical curves describing the BF_4^- reorientation) is subtracted from the measured values. This is a good approximation of the paramagnetic relaxation contribution caused by unpaired electrons. (▽): ^{19}F T_1 at 29.0 MHz, cooling direction; (▲): ^{19}F T_1 at 29.0 MHz, heating direction; (○): ^{19}F T_1 at 83.5 MHz, cooling direction; (◇): ^{11}B T_1 at 29.0 MHz, cooling direction.

3.2 [Fe(ptz)$_6$](BF$_4$)$_2$

The recovery of the longitudinal ^{19}F and ^{11}B magnetization was exponential in the whole temperature range. The relaxation time curves (Figs. 3–5) tend to decrease with decreasing temperature above 130 K because of the local magnetic fields of the high-spin state electron structure of the Fe$^{\mathrm{II}}$ ions. According to the high spin fraction *vs.* temperature curve $\gamma(T)$ [1–4], the predominant majority of the Fe$^{\mathrm{II}}$ ions changes its spin state within a few tenths of kelvins. This process has a wide hysteresis as it can be seen in Figures 4 and 5 and as others reported it [1–4]. The remaining high-spin (or low-spin) state part undergoes the spin transition in a wider temperature range. Our ^{19}F and ^{1}H [6,10] relaxation time data reflect the same $\gamma(T)$ till 100 K where they reach the T_1 values measured for [Zn(ptz)$_6$](BF$_4$)$_2$ (Fig. 3).

Above 100 K, [Fe(ptz)$_6$](BF$_4$)$_2$ can be treated as a diamagnetic system containing paramagnetic (high-spin state Fe$^{\mathrm{II}}$) ions. For such systems, Bloembergen introduced the theory of spin-lattice relaxation *via* paramagnetic ions [12]. According to this model, the relaxation is due to two mechanisms: electron relaxation and spin diffusion (paths 3 in Fig. 1). There are different limiting cases characterized by the ratio of relaxation rates for the two mechanisms. For the description of ^{1}H spin-lattice relaxation *via* paramagnetic ions, we applied [10] the rapid diffusion limiting case derived by Lowe and Tse [13]. For the ^{19}F nuclei, the diffusion-limited case is the appropriate one since they are not in chemical connection with the paramagnetic Fe$^{\mathrm{II}}$ ions and so the spin diffusion cannot be powerful.

In the limiting case of rapid diffusion, T_1 is given by the equation

$$T_1 = \frac{3b^3}{4\pi N_{\mathrm{p}} \overline{C}}, \tag{7}$$

where b is the "barrier radius", inside of which spin diffusion is not possible because the local field of the paramagnetic ion has shifted the resonance of nuclei sufficiently far from the other nuclei so that the spin-flip mechanism (which requires both nuclei to have the same resonance frequency) is quenched. $N_{\mathrm{p}} = N(T)\gamma_{\mathrm{HS}}(T)$ is the concentration of high-spin state Fe$^{\mathrm{II}}$ ions, $N(T)$ is the number of Fe$^{\mathrm{II}}$ ions per unit volume. $\overline{C}$ is given by

$$\overline{C} = \frac{2}{5}\left(\frac{\mu_0 \hbar}{4\pi}\right)^2 S(S+1)\gamma_{\mathrm{S}}^2\gamma_{\mathrm{I}}^2 \frac{\tau_{\mathrm{c}}}{1+\omega_{\mathrm{I}}^2\tau_{\mathrm{c}}^2}\cdot \tag{8}$$

γ_{S} and γ_{I} are the magnetogyric ratios of the paramagnetic ion and nucleus I, respectively. S is the spin of the paramagnetic ion. $\tau_{\mathrm{c}} = \tau_0 \mathrm{e}^{E_{\mathrm{a}}/RT}$ is the correlation time of the z component of the paramagnetic-ion spin, and $\omega_{\mathrm{I}} = \gamma_{\mathrm{I}} B_0$.

In the diffusion-limited case, T_1 is given by

$$T_1 = \frac{3}{8\pi N_{\mathrm{p}} \overline{C}^{1/4} D^{3/4}}, \tag{9}$$

where $D \propto T_2^{-1}$ is the spin diffusion coefficient.

The measured ^{19}F spin-lattice relaxation times consist of a dipolar and a paramagnetic part ($T_{1,\text{meas.}}^{-1} = T_{1,\text{dip.}}^{-1} + T_{1,\text{param.}}^{-1}$). Equation (9) corresponds to $T_{1,\text{param.}}$. The dipolar relaxation mechanisms are exclusively determined by the reorientations of the molecular groups. The paramagnetic relaxation mechanism has an effect on the measured T_1 values as an additional perturbation. Therefore the dipolar part can be estimated by theoretical curves of the BF_4^- reorientation described in Section 3.1. For the fitting of equation (9) to the temperature range between 130 and 300 K, $\tau_c = 1.0\times10^{-13}\exp(3.0\times10^3/RT)$ s obtained previously [10] was used. $N(T)$ was calculated from crystallographic cell parameters in reference [14]. $\gamma_{HS}(T)$ was taken from reference [4]. T_2 was estimated with the reciprocal of the ^{19}F line width at half maximum (the results of the spectrum measurements will be published separately). The remaining constant parameters were treated as a single variable fitting parameter. The resulting curves are shown in Figure 5. The rapid diffusion model gives curves with steeper slope and no frequency dependence in this temperature region and so it is not the appropriate limiting case for the ^{19}F nuclei.

The relaxation time *vs.* temperature curves of the two compounds are expected to be almost the same below 100 K since a 100% spin transition is suggested [1–4]. The magnetic moment of $[Fe(ptz)_6](BF_4)_2$ is smaller than 0.01 emu/g = 15 A/m between 55 and 85 K, *i.e.* it is negligible compared to the maximal magnetic moment of 2 emu/g = 2 600 A/m at $T = 135$ K [15]. Essentially the same T_1 minima were found between 55 and 85 K as for $[Zn(ptz)_6](BF_4)_2$ (^{19}F at 83.5 MHz and 29.0 MHz data, ^{11}B at 29.0 MHz data), thus each can be assigned to the reorientation of the BF_4^- anions. This anion motion can be described by activation energy and correlation time values very close to the ones calculated for the zinc complex (see Tab. 1). On the basis of the direct correlation between the dynamics of the two compounds shown by ^1H [10], ^{11}B and ^{19}F T_1(T) curves in the quasi diamagnetic temperature region of the iron complex and since the complexes are isomorphic, we assume that the same types of molecular reorientations are present in both compounds in the high-temperature region, too. As a consequence, we suggest that the changes of the dynamical structure occurring at 130–140 K (see previous section) triggers the spin transition determining its temperature ($T_{1/2}$). Nagai *et al.* [8] got also to this conclusion by the analysis of their 2D-ACAR measurements on $[Zn(ptz)_6](BF_4)_2$ and $[Fe(ptz)_6](BF_4)_2$ single crystals.

^{19}F and ^1H relaxation times are much smaller for $[Fe(ptz)_6](BF_4)_2$ than for $[Zn(ptz)_6](BF_4)_2$ and they have a V-shaped minimum below 50 K (Fig. 3). The faster relaxation can originate from very low concentration residual high-spin state Fe^{II} ions and the later was attributed to some magnetic interactions involving clusterization[1] between them [10].

[1] Magnetic moment measurements made by a SQUID equipment suggest a cluster formation process among the residual high-spin state Fe^{II} ions between 1.8 and 20 K [15].

4 Conclusions

^{19}F and ^{11}B spin-lattice relaxation time measurements for $[Zn(ptz)_6](BF_4)_2$ and for the spin-crossover compound $[Fe(ptz)_6](BF_4)_2$ showed that BF_4^- anion reorientation is active in both compounds above 50 K. For $[Zn(ptz)_6](BF_4)_2$, the anion-reorientation dynamics was found to be different at 50–90 K, 90–120 K, and 150–300 K. It changes rapidly between 120 and 150 K: even small changes in the lattice parameters activate different reorientational motions. Since the Zn^{II} and the Fe^{II} compounds are isomorphic and the same molecular motions were found in both compounds at low temperatures, the reorientation dynamics is expected to be almost identical in the higher-temperature region, too. The later assumption makes possible to draw the conclusion, that the process of continuously changing anion and propyl chain reorientation dynamics is also present in the Fe^{II} compound between 120 and 150 K. Since the spin transition temperature of the Fe^{II} compound is 128 K (cooling direction), we suggest that the changes of the lattice dynamics and the parameters determining the spin transition temperature are interdependent.

Thanks are due to P. Bánki for his help with the experiments. Part of the work was supported by Grants T016670 of the Hungarian Science Foundation (OTKA), FKFP-0148/1997 of the Hungarian Ministry of Culture and Education and AKP 97-33 of the Hungarian Academy of Sciences.

References

1. P. Gütlich, A. Hauser, H. Spiering, Angew. Chem. Int. Ed. Engl. **33**, 2024 (1994).
2. P.L. Franke, J.G. Haasnoot, A.P. Zuur, Inorg. Chim. Acta **59**, 5 (1982).
3. E.W. Müller, J. Ensling, H. Spiering, P. Gütlich, Inorg. Chem. **22**, 2047 (1983).
4. S. Decurtins, P. Gütlich, K.M. Hasselbach, A. Hauser, H. Spiering, Inorg. Chem. **24**, 2174 (1985).
5. L. Wiehl, H. Spiering, P. Gütlich, K. Knorr, J. Appl. Cryst. **23**, 151 (1990).
6. M. Bokor, T. Marek, K. Tompa, A. Vértes, J. Mol. Struct. **410–411**, 1 (1997).
7. T. Marek, M. Bokor, K. Tompa, Gy. Lasanda, L. Párkányi, J. Buschmann, J. Phys. Chem. Solids (in press).
8. Y. Nagai, H. Saito, K. Süvegh, Phys. Rev. B **57**, 14119 (1998).
9. P. Poganiuch, S. Decurtins, P. Gütlich, J. Am. Chem. Soc. **112**, 3270 (1990).
10. M. Bokor, T. Marek, K. Tompa, J. Mag. Reson. A **122**, 157 (1996).
11. S. Albert, H.S. Gutowsky, J. Chem. Phys. **59**, 3585 (1973).
12. N. Bloembergen, Physica **15**, 386 (1949).
13. I.J. Lowe, D. Tse, Phys. Rev. **166**, 279 (1968).
14. L. Wiehl, Acta Crystallogr. B **49**, 289 (1993).
15. L. Kiss *et al.*, Chem. Phys. Lett. (to be published).